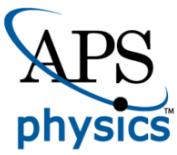

Curvature-driven foam coarsening on a sphere: A computer simulation

Shawn D. Ryan, Xiaoyu Zheng, and Peter Palffy-Muhoray

Phys. Rev. E **93**, 053301 — Published 9 May 2016

DOI: 10.1103/PhysRevE.93.053301

Curvature driven foam coarsening on the sphere: a computer simulation

Shawn D. Ryan,[1,2] Xiaoyu Zheng,[1] and Peter Palffy-Muhoray[2]

[1] *Department of Mathematical Sciences, Kent State University, Kent, OH 44240, USA*
[2] *Liquid Crystal Institute, Kent State University, Kent, OH 44240, USA*

(Dated: April 19, 2016)

The von Neumann-Mullins law for the area evolution of a cell in the plane describes how a dry foam coarsens in time. Recent theory and experiment suggest that the dynamics are different on the surface of a three-dimensional object such as a sphere. This work considers the dynamics of dry foams on the surface of a sphere. Starting from first principles, we use computer simulation to show that curvature driven motion of the cell boundaries leads to exponential growth and decay of the areas of cells, in contrast to the planar case where the growth is linear. We describe the evolution and distribution of cells to the final stationary state.

I. I. INTRODUCTION

A foam is a gas-liquid mixture consisting of pockets of gas separated by thin films of liquid. Foams abound in daily life, from soap bubbles and waves breaking on a beach to whipped cream and the chemical foam of a fire extinguisher. This work focuses on the phenomenon of foam coarsening, where the bubble size and shape change over time. Interest in this phenomenon extends beyond conventional foams. The same two- or three-dimensional polyhedral structures separated by well-defined boundaries can be seen in many materials such as polycrystalline alloys, ceramics, lipid monolayers, and garnet films [1]. The study of these domains can extend beyond simple materials to biology (e.g., cornea in an eye [2]) or cosmology (e.g., voids in the universe [3]). For a general review of foams see [4].

The von Neumann law describing foam coarsening has been regarded as a historical touchstone at the interface of mathematics and materials science [5]. In 1952, von Neumann showed that, in the plane, the rate of change of the area of a given cell is independent of the cell size, but rather depends solely on the number of its edges [6]. In the original von Neumann model, the evolution of the cell is due to gas transfer across cell walls (cell edges in 2D) between neighboring cells. The rate of gas transfer is assumed to be proportional to the pressure difference Δp across a cell edge. In equilibrium, according to the Young-Laplace law,

$$\Delta p = -\gamma \kappa_g, \tag{1}$$

the pressure difference is proportional to curvature κ_g of the edge and γ is the surface tension. The curvature κ_g is then constant along each edge. Thus, the rate of change of area for a given cell is

$$\frac{dA}{dt} = -\mu_0 \gamma \int_{\partial A} \kappa_g ds = -\mu_0 \gamma \sum_i \kappa_g(i) L_i, \tag{2}$$

where μ_0 is the permeability and L_i are the lengths of the edges around the boundary ∂A of the cell [7]. The integral on the righthand side can be computed as

$$\sum_i \kappa_g(i) L_i = 2\pi - \sum_{i=1}^{n} (\pi - \theta_i), \tag{3}$$

where θ_i is the interior angle at the ith vertex. If the vertices are triple junctions, then $\theta_i = 2\pi/3$ according to Plateau's Law. From this we recover von Neumann's result

$$\frac{dA_n}{dt} = K_0 (n-6), \tag{4}$$

where $K_0 = \pi \mu_0 \gamma / 3$. Commonly referred to as the "$n-6$" rule this equation shows that cells with greater than six sides grow linearly while cells with less than six sides decay in time. A cell with six sides might change its shape, but the area would remain constant. **Cells with less than six sides disappear by shrinking and the number of cells steadily decreases. Foams where all the cells are hexagon can last, but they are metastable, in the sense that any topological change would create at least one cell with less than six sides, and coarsening would start.** There are **five basic approaches** that have been used to model foam coarsening in 2D: Direct Simulation [7–11], Vertex Models [12–16], Mean-field theory [17, 18], **Potts Model [19–22], and the surface evolver [23–25]**. A summary can be found in the review article [1].

The direct approach attempts to reproduce the equilibrium configuration at each time step by including the essential physics of gas diffusion and boundary motion [8, 9, 26]. There have been other direct numerical methods specifically developed for foam coarsening **including the surface evolver [27–29]**. Another type of direct simulation is the vertex approach where the focus is on getting the vertices to move correctly and assuming the cell boundaries will evolve instantaneously fast to their equilibrium positions (e.g., [12–16]). In contrast to a direct approach, one can also study the dynamics of a distribution function $\rho = \rho(n, A, t)$ using a PDE approach (e.g., [1, 17, 18]). The final approach uses the Potts model [30–32], which takes a microscopic perspective where **"lattice sites"** can move from cell to cell,

thereby changing its area, in order to minimize a surface energy Hamiltonian [19–22].

The first generalization of the von Neumann law to non-planar surfaces with Gaussian curvature κ was carried out in [33]. Using the Gauss-Bonnet theorem (5),

$$\int_A \kappa dA + \int_{\partial A} \kappa_g ds + \sum_{i=1}^{n} (\pi - \theta_i) = 2\pi, \tag{5}$$

where κ_g is the geodesic curvature, constant along each edge, Eq. (2) becomes,

$$\frac{dA}{dt} = K_0 \left[(n-6) + \frac{3}{\pi} \int_A \kappa dA \right] = K_0 \left[(n-6) + \frac{3A}{\pi} \right]. \tag{6}$$

The last equation holds only for the sphere of unit radius and K_0 contains the relevant physical parameters [33, 34]. The dependence of the rate of change of the area of a cell on its size, in addition to the number sides, fundamentally changes the dynamics. Sufficiently large cells will continue to grow, while a small cell with less than six sides can either grow or shrink depending on its area. In fact, there is no stable configuration other than for a single cell to enclose the entire surface of the sphere. **Recall that on a sphere there should be a non-zero topological charge, so that it is impossible to have a sphere only with hexagons [4].**

Recently, an experiment was carried out by Roth et al. [34] to study the evolution of a dry foam between two hemispherical domes. They observed that a cell with six sides was not stable, unlike in the planar case, but instead grew at a rate dependent on the cell size. Other experiments investigating foam coarsening in 2D and quasi-2D can be found in [35, 36].

The remainder of the paper is organized as follows. In Section II, a mathematical model describing the curvature driven dynamics of a foam on a smooth non-planar surface is derived from energy minimization, using a variational approach. Here the curvature is allowed to vary along each edge. The resulting equation of motion for the cell area is the same as in [33]; however, it is not restricted to uniform curvature along cell edges. The model predicts exponential growth/decay of cells in time for general smooth surfaces. In Section III, a numerical scheme is proposed to simulate the foam coarsening on the surface of a sphere through curvature driven dynamics. In Section IV, exponential growth of each individual cell is demonstrated and the longtime behavior is described via computer simulations.

II. II. MODEL

The foam evolution process involves the continuous motion of edges and vertices, interrupted by rare events of topological changes, **such as neighbor swapping (T1) or the disappearance of cells (T2) [4, 37]**, at discrete time instances elaborated on in Sect. III. In this section, we focus on constructing the mathematical model describing the continuous aspects of the evolution. The dry foam considered is a region on a surface or an entire bounded surface composed of disjoint cells separated by piecewise smooth boundaries or cell edges, which meet at triple junctions. The edges are assumed to have zero thickness. We construct the dissipative dynamics of cells using a generalized Lagrangian approach.

A cell edge at a time t can be described by its position vector $\mathcal{R}(s,t)$ parametrized by arclength s, $0 < s < L(t)$, where $L(t)$ is the length of the edge. The total energy of the foam is taken to be the sum of the interfacial energies of all edges, given by

$$E(t) = \sum_i \int_0^{L_i} \gamma ds, \tag{7}$$

where γ is the line tension (surface tension times the height of the foam above the surface). We assume that inertial effects are negligible, and the drag per length on a moving edge is proportional to its velocity. The drag force on the vertex, which has zero length, is zero. Without external forces, we assume that the loss of energy is due only to the viscous dissipation, then

$$\frac{dE}{dt} = -\sum_i \int_0^{L_i} \frac{1}{2} \eta \dot{\mathcal{R}}^2 ds. \tag{8}$$

where η is the viscosity. After a straightforward variational calculation, the equation of motion of a point on an edge is

$$\dot{\mathcal{R}} = \frac{\gamma}{\eta} \frac{\partial^2 \mathcal{R}}{\partial s^2} \left(\mathbf{I} - \hat{\mathbf{N}}\hat{\mathbf{N}} \right), \tag{9}$$

where $\hat{\mathbf{N}} = \nabla\psi/|\nabla\psi|$ is the unit normal to the surface, and $\psi(\mathcal{R}) = 0$ defines the surface. Thus each point on an edge moves at a speed proportional to its local geodesic curvature, in the direction of $\frac{\partial^2 \mathcal{R}}{\partial s^2}$ projected onto the surface[1]. The variational calculation also obtains the Herring condition

$$\gamma \sum_{k=1}^{K_j} \frac{\partial \mathcal{R}_k}{\partial s}(\mathbf{v}) = 0, \tag{10}$$

where K_j is number of junctions at a vertex $\mathbf{v}$. These are also boundary conditions of Eq. (9); the line tensions from all edges at a vertex add to zero, and hence the vertices are always in mechanical equilibrium. In the typical triple junction case, this implies that the angle between the two unit tangents is $2\pi/3$.

The rate of change of the area of a cell can now be computed; since

$$\frac{dA}{dt} = \sum_{i=1}^{M} \oint_{\partial A} \left(\frac{\mathcal{R}_i}{|\mathcal{R}_i|} \times \dot{\mathcal{R}}_i \right) \cdot d\mathcal{R}_i, \tag{11}$$

[1] A similar result has been obtained by Mullins [38] considering local curvature driven motion of metal grains in the plane.

substituting Eq. (9) gives

$$\frac{dA}{dt} = \frac{\gamma}{\eta}\sum_{i=1}^{M}\oint_{\partial A}\left(\frac{\mathcal{R}_i}{|\mathcal{R}_i|}\times\frac{\partial^2\mathcal{R}_i}{\partial s^2}(\mathbf{I}-\hat{\mathbf{N}}\hat{\mathbf{N}})\right)\cdot d\mathcal{R}_i. \quad (12)$$

We note that the integrand in Eq. (12) is just the signed geodesic curvature along the cell edges. Assuming that the angle at each vertex is $2\pi/3$, (i.e. triple junctions at the vertices), the Gauss-Bonnet theorem gives at once

$$\frac{dA}{dt} = \frac{\gamma}{\eta}\left[\frac{\pi}{3}(n-6)+\int_A \kappa dA\right]. \quad (13)$$

This is more general than the result in [33], which requires that the geodesic curvature κ_g be a constant along cell edges. Eq. (13) is valid up to a topological change when the number of sides n of a cell changes. **We note that if** $\kappa = 0$, the growth/decay is linear in time, consistent with the planar case. Our interest in this work is to study the nonlinear dynamics where $\kappa \neq 0$ as on the surface of a sphere.

In particular, for the case of a sphere with radius R_0, $\psi(\mathcal{R}) = \mathcal{R}\cdot\mathcal{R} - R_0^2$, the Gaussian curvature of the surface is a constant, $\kappa = 1/R_0^2$, and the equation of motion for each edge point becomes

$$\dot{\mathcal{R}} = \frac{\gamma}{\eta}\left[\frac{\partial^2\mathcal{R}}{\partial s^2}(I-\frac{1}{R_0^2}\mathcal{R}\mathcal{R})\right]. \quad (14)$$

The rate of change of area of each cell is then

$$\frac{dA}{dt} = \frac{\gamma}{\eta}\left[\frac{\pi}{3}(n-6)+\frac{A}{R_0^2}\right]. \quad (15)$$

We non-dimensionalize by scaling all lengths by the sphere radius R_0 and all times by the characteristic time $\eta R_0^2/\gamma$ as in [28]. Using these quantities, in dimensionless units,

$$\frac{d\tilde{A}}{d\tilde{t}} = \frac{\pi}{3}(n-6)+\tilde{A}. \quad (16)$$

For a cell with n sides, if $n \geq 6$, the area will increase until a topological change occurs. If $n < 6$, the cell area remains stationary only if $\tilde{A} = \frac{\pi}{3}(6-n)$; any perturbation will make it unstable. In the longtime limit, the only stable configuration will be one where no edges remain, and one cell covers the entire sphere. Given an initial area $\tilde{A}_0$ of a cell, and its number of sides n, solving Eq. (16) for $\tilde{A}$ gives the explicit expression for the area evolution,

$$\tilde{A}(\tilde{t}) = \left[\tilde{A}_0+\frac{\pi}{3}(n-6)\right]e^{\tilde{t}} - \frac{\pi}{3}(n-6). \quad (17)$$

We expect exponential growth/decay of cells on the sphere, as opposed to planar case, where the growth is linear in time. An indication of exponential growth may be seen in the quotient $Q := \ddot{A}/\dot{A}$. On a sphere, we expect $Q = 1$, while on the plane we expect $Q = 0$.

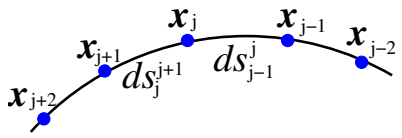

FIG. 1. Illustration of edge discretization. For $t > 0$, the spacing of the edge points is non-uniform ($ds_j^{j+1} \neq ds_{j-1}^{j}$).

III. III. NUMERICAL IMPLEMENTATION

In this section, we present in detail the steps by which the simulations were carried out on the surface of the sphere: **the initialization**, the discretization procedure for the cell edges, the evolution of the edges and vertices, the numerical computation of cell area, and **we end with a discussion** of the topological changes that occur in the long time. The surface of the sphere differs from a planar surface in that the whole surface is bounded, and there is no physical boundary, thus there is no need to impose any boundary conditions. In recent years many numerical methods have been developed for simulating the motion of boundary curves on surfaces; see [39] for an overview. Here we take a first principles approach relying on kinetic equations of motion to evolve the edges.

Initialization. It is convenient to consider an initial distribution of cells generated from a Voronoi diagram on the unit sphere. The cells are generated from N randomly placed nodes on the surface using an analog of the plane sweep "Fortune" algorithm [40]. The cells in this Voronoi diagram are made up of vertices and a set of edges connecting each vertex to three others (see Figure 4). The cell edge connecting vertex $\mathbf{v}_i$ to vertex $\mathbf{v}_j$ is made up of a great circle of length $\ell_{ij} = \arccos(\mathbf{v}_i\cdot\mathbf{v}_j)$. This edge is then discretized into $M_{ij} = \lceil \ell_{ij}/dx \rceil$ edge points. The k^{th} point on an edge can be computed by

$$\mathbf{x}_{ij}^k = \mathbf{u}\cos(kdx) + \mathbf{w}\sin(kdx), \quad (18)$$

for $k = 1, ..., M_{ij}-1$, where $\mathbf{u} = \mathbf{v}_i$ and $\mathbf{w} = [(\mathbf{v}_i\times\mathbf{v}_j)\times\mathbf{v}_i]/\|\mathbf{v}_i\times\mathbf{v}_j\|$.

There are two types of points in the system: edge points $\{\mathbf{x}\}$ that evolve via curvature driven motion and vertices $\{\mathbf{v}\}$ that must satisfy the Herring condition. Once all the cell boundaries are discretized we say a vertex $\mathbf{v}$ satisfies the Herring condition if the great circles from $\mathbf{v}$ to each of its neighbors meet at an angle $\theta = 2\pi/3$. The dynamics of the foam is initiated by vertex movement to satisfy Herring condition, followed by the motion of edge points driven by a modified curvature caused by the new vertex location. The dynamics proceeds by repeated updates of the vertices and edge points.

Algorithm. A step-by-step procedure for the evolution of the system in a given time step is outlined below.

> *Step 1:* Each vertex is moved to the point satisfying the Herring condition, Eq. (10), using a fixed point iteration (e.g., see Appendix A and Eq. (A1)) for a given tolerance ϵ.

Step 2: Each of the points along the cell edge are evolved via curvature motion on the surface of the sphere using a standard Forward Euler scheme to solve the non-dimensional form of Eq. (14)

$$\mathbf{x}(t+dt) = \mathbf{x} + dt(\boldsymbol{\kappa}_0 - (\boldsymbol{\kappa}_0 \cdot \mathbf{x})\mathbf{x}), \tag{19}$$

where $\boldsymbol{\kappa}_0 = \frac{\partial^2 \mathcal{R}}{\partial s^2}\Big|_{\mathbf{x}}$. A three-point stencil $\boldsymbol{\kappa}_0$ can be approximated as

$$\boldsymbol{\kappa}_0 = \frac{2\mathbf{x}_{j+1}ds_{j-1}^j - 2\mathbf{x}_j(ds_{j-1}^j + ds_j^{j+1}) + 2\mathbf{x}_{j-1}ds_j^{j+1}}{ds_j^{j+1}ds_{j-1}^j(ds_{j-1}^j + ds_j^{j+1})}, \tag{20}$$

where $ds_{j-1}^j = \arccos(\mathbf{x}_{j-1}\cdot\mathbf{x}_j)$ and $ds_j^{j+1} = \arccos(\mathbf{x}_j \cdot \mathbf{x}_{j+1})$. Observe that if the mesh is uniform (e.g., $ds_{j-1}^j = ds_j^{j+1}$), then this reduces to the standard second order finite difference scheme (see Fig. 1).

Step 3: Once the set of new points $\{\mathbf{x}_j(t+dt)\}$ is computed we project the result back onto the sphere, $\hat{\mathbf{x}}_j = \mathbf{x}_j/\|\mathbf{x}_j\|$.

Step 4: Check for any topological changes that need to be resolved. Return to *Step 1.*

To evolve the edge points efficiently and accurately, we paid special attention to the discretization as elaborated on below. One example is the use of a temporal adaptive mesh. In order for the system to evolve via curvature motion an edge must have at least one additional point beyond the two vertices to use the three-point stencil, Eq. (20). Thus, in systems with many cells initially, two of the vertices may be very close. The global spatial discretization dx should be chosen so that the geodesic distance between the two vertices $\arccos(\mathbf{v}_1\cdot\mathbf{v}_2) > 2.5dx$. The adverse effect of a small dx at the beginning of the simulation is a small dt, which is $O(dx^2)$. Once cells start to be removed this fine discretization is no longer needed so one can coarsen the system by doubling dx, therefore quadrupling dt. Specifically, we check, after a set time period, the condition that the minimal number of discretized points along any edge is 5. If this is the case we take the set of points along each edge keeping every other point and each vertex. In the simulations presented we restrict $dx_{max} < 0.02$ to ensure that we do not sacrifice accuracy for speed. Therefore, early on, before the small cells are removed, we have a fine mesh, and as the foam coarsens, we speed up the simulation.

The other example is maintaining a roughly spatially uniform mesh at each time step for better global accuracy on approximating the curvature. Throughout the course of evolution, the edge points get closer and further apart. To resolve the curvature reasonably well we wish to stay near a uniform mesh by imposing a condition on the edge points using the global mesh size dx, $.5dx < ds_j^{j+1} < 1.5dx$. If two points are closer than $0.5dx$, we remove both points and replace them with a single point at the midpoint of the great circle connecting them as in [7]. If two points are a greater distance than $1.5dx$, then we add an additional point at the midpoint along the great circle. This ensures that locally the mesh remains nearly uniform.

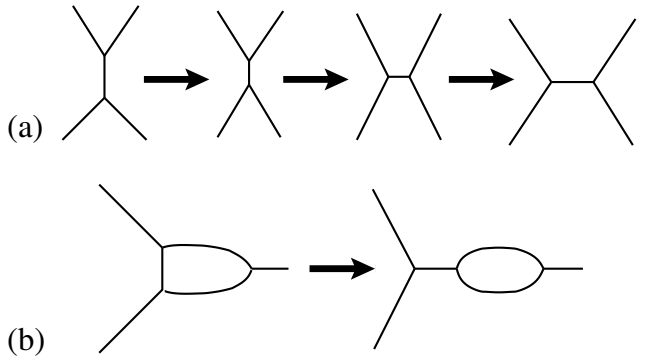

FIG. 2. (a) A boundary flip occurs when one edge becomes very short, it is rotated by $\pi/2$. (b) For 3-sided cells the boundary flip results in a diangle.

To keep track of the area of each cell, we approximate the area by considering each cell as a spherical $\mathcal{N}$-gon, where $\mathcal{N}$ is the total number of unique discretized edge points around its boundary. The area of a spherical polygon is $A = \sum_{i=1}^{\mathcal{N}} \alpha_i - (\mathcal{N}-2)\pi$ where α_i are the interior angles of the polygon [41].

Topological Changes. To study the longtime dynamics of cells, the model must address critical events which occur throughout the course of the evolution. When a cell boundary becomes very small one of two events can occur: (i) Boundary flipping (T1) or (ii) Cell removal (T2) as in [4, 15, 17, 37].

The former is implemented in the simulation when an edge has a length less than $1.5dx$. There are no longer enough edge points to evolve the boundary via curvature motion and this small edge is only composed of two vertices. One can think of two cells being forced together and pinching the space out between them (see Fig. 2). To remedy the situation, the two vertices are rotated about their midpoint by an angle of $\pi/2$ and connected to one former neighbor and one new neighbor. **In general, the rotation angle may differ from $\pi/2$, but here it is assumed for simplicity.** Immediately after the vertices will begin to move apart due to the Herring condition. We note that after a boundary flip two cells gain a side and two cells lose a side.

In the latter case, when a cell area becomes small (e.g., $A < 5dx^2$) the cell must be removed. As in [15] and consistent with cell growth and decay in our system, only two, three, and four-sided cells are removed while cells of five or more sides execute a boundary flip to reduce the number of sides before removal. If a cell has four sides, then the four vertices are removed and replaced by two triple junctions satisfying the Herring condition. In this case, two cells lose a side and two cells maintain the same number of sides. Next, if a cell has three sides it shrinks to a point. The three vertices composing the cell are removed and one new vertex appears connected to the remaining neighboring vertices. Each of the neighboring cells has a net loss of one side. If a cell has two sides, when the area becomes small, the two edges connecting the two

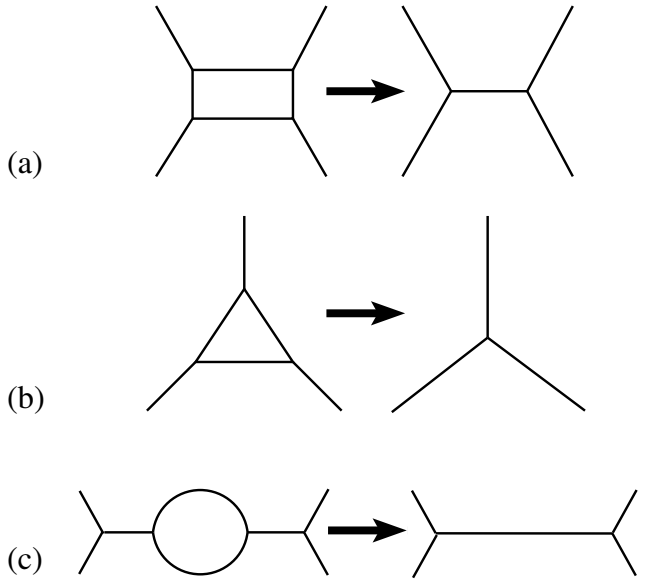

FIG. 3. (a) For 4-sided cells all vertices are removed and replaced by two new vertices forming triple junctions. (b) For 3-sided cells all vertices are removed and replaced by one new vertex. (c) For 2-sided cells the edges are removed and the vertices become interior edge points.

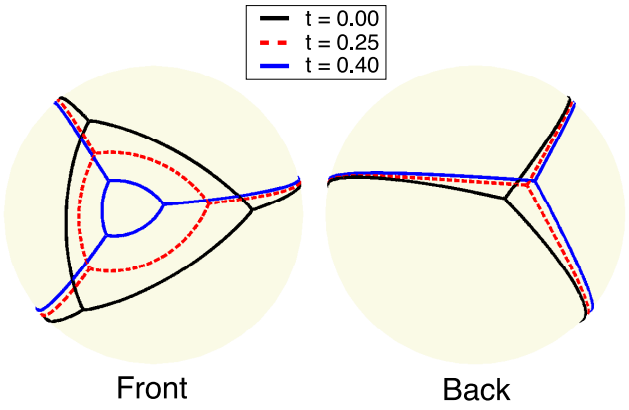

FIG. 4. Evolution of one realization of the 4 cell case at three instances in time. The smallest cell in front shrinks exponentially fast.

vertices are removed and these vertices become interior points on the edge. Fig. 3 illustrates each event. **In simulation we have observed the removal of two-, three-, and four-sided cells.** After each topological event, the number of sides change on the cells involved, altering their dynamics in time according to Eq. (13).

There are a few interesting cases to consider to clarify the numerical implementation. One occurs when a 3-sided cell has only one short side requiring a boundary flip, yet its area is not small enough to be removed. The boundary flip is carried out resulting in a diangle (e.g., see Fig. 2), **which has been observed in our simulations**. The edges of such a cell still evolve via curvature motion and the evolution of the area obeys Eq. (16). Another scenario is when two edges on the same cell become small enough to flip within the same time step. In fact, the first edge which meets the criterion for flipping is flipped. All other flips that would involve one of the two vertices that have just moved are suspended until the next time step, when the conditions for flipping can be checked.

Our algorithm allows the use of GPUs for faster computations. We use a hybrid CPU/GPU scheme where the vertex and edge evolution are carried out in parallel on the GPUs while the topological changes and area computation are done on the CPU. Each GPU core handles the dynamics of a vertex and up to three adjoining edges (each edge is assigned to only one GPU) and executes the computations in parallel. We find the efficiency in using GPUs increases with the number of vertices. In the case of a 20 cell simulation (36 vertices using 36 simultaneous GPU cores) the simulation time decreased on average by a factor of four compared to the same code run only on the CPU. **For 100 cells, as in Figure 6, the typical simulation will run for around 4 hours on an Nvidia Tesla C2075 GPU with 512 cores.** The overall efficiency decreases in time due to the fact that cells are removed resulting in a decrease in the number of vertices.

IV. IV. RESULTS AND DISCUSSION

In this section the focus is verifying the effective von Neumann law on the sphere, Eq. (16), through numerical simulation, and study longtime dynamics. To provide insight into our numerical algorithm, we consider the test case of four cells on the sphere, each with three sides, and study the evolution of these cells until the first topological change. Fig. 4 shows the evolution of one realization of the four cells at three instances of time from two different perspectives. The smallest cell on the front shrinks the fastest.

In Fig. 5a, we show the cell area from numerical simulation using $dx = 0.0125$ together with the analytic solution from Eq. (17) for the purpose of comparison; they are in close agreement. Convergence study shows that the numerical algorithm presented here, combining the curvature driven edge point evolution and fixed point iteration for vertex evolution, is first order accurate in dx, due to the fact that the convergence rate of the vertex calculation is first order as we vary dx.

To provide evidence of exponential growth, we consider the quotient $Q := \ddot{A}/\dot{A}$. To avoid effects of numerical noise, we consider the nonlocal version of this quotient, similar to the approach in [15]

$$Q := \frac{2[A(t+T) - 2A(t) + A(t-T)]}{T[A(t+T) - A(t-T)]}, \qquad (21)$$

where $T = Mdt$ is a scaled time interval. As $T \to 0$

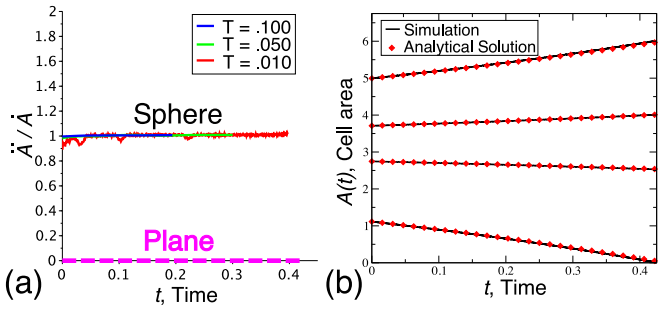

FIG. 5. (a) Area evolution in the case of 4 cells. The curves correspond to the different cells. (b) The quotient $Q := \ddot{A}/\dot{A}$ averaged over all the 4 cells. Exponential growth is seen in contrast to linear growth in the planar case. Each color represents a different time interval T in the computation of the "non-local" quotient.

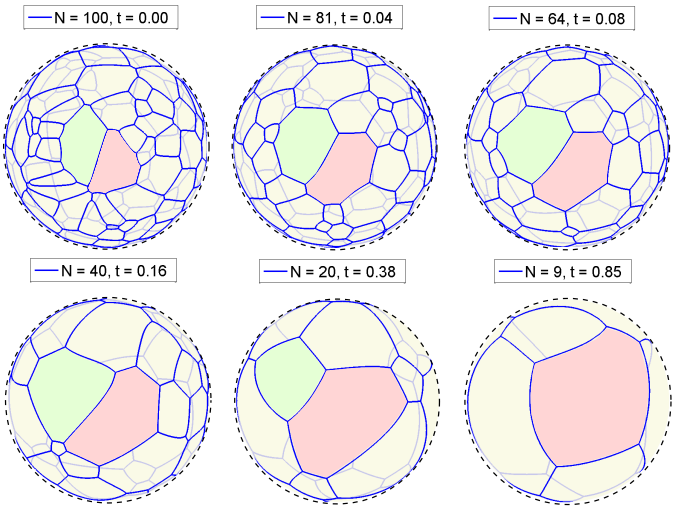

FIG. 6. Foam coarsening over time starting from an initial distribution of 100 cells. Red and green cells each start with nine sides. Spheres are made transparent to allow for viewing all cells at once. **See Supplementary Material at [42] for the corresponding movie**.

Eq. (21) recovers the pointwise definition of the quotient of derivatives. Our simulations show that $Q \approx 1$ for the case of four initial cells, verifying exponential growth as shown in Fig. 5b. Similar behavior is observed for larger initial cell numbers (e.g., $N = 20, 50, 100, 200$). Since the numerical results capture the exponential growth as well as quantitatively match the area evolution, our numerical scheme is apparently robust for simulation of the long-time evolution of the foam on the surface of the sphere.

Next, we investigate how the distribution of cells evolves in time. **Our simulations show foam coarsening, where the number of cells decreases and the average area of the remaining cells grows in time, as can be seen in Fig. 6, until only a single cell remains enclosing the entire surface of the sphere.**

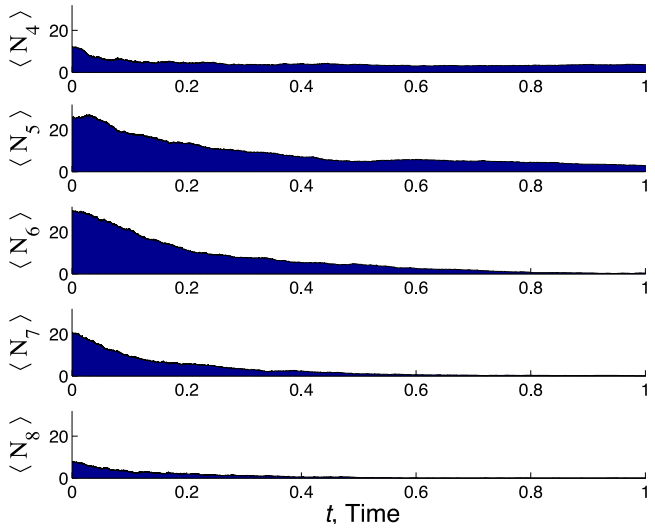

FIG. 7. Numbers of cells $\langle N_i \rangle$ with given number i of vertices averaged over 20 simulations as function of time.

There are several interesting aspects of the statistics of cell evolution. One is the dependence of the cell distribution on the number of sides/vertices as function of time. Fig. 7 shows the numbers of cells with a given number of vertices as function of time. Initially, the most prevalent cells are those with 6 vertices; this gradually shifts to cells with fewer vertices. Fig. 8 shows that initially there are many small cells; the peak of the histogram is centered around $n = 6$ consistent with the planar case [7, 15, 16]. As the system evolves and cells begin to disappear, the peak shifts towards cells with smaller numbers of sides. In addition, one can consider the distribution of cell areas (not shown). Initially this distribution is nearly Gaussian, with mean area $4\pi/N$. As the foam coarsens and time evolves, this distribution broadens with the mean shifting towards larger values of the average area.

The simulations also reveal that the cell which is most likely to survive to the end is the cell is the one with the largest number of sides. As an example shown in Fig. 6, the two cells colored in green and red, initially with 9 vertices, persist for a long time, while small cells in the vicinity with smaller numbers vertices disappear quickly. In particular, if towards the end of the simulation all the cells have the same numbers of sides (e.g., four 3-sided cells remain, as in Fig. 4), the one with the largest area will survive longest. This continues until the final stages of the simulation, where there are three diangles remaining until one disappears. What remains then is a closed curve on the sphere, corresponding to two cells, with two cell faces, two vertices and two edges. The edges continue to evolve via curvature motion until the small cell shrinks to a point, leaving one vertex, one cell face, and no edges.

Finally, we consider the total number of cells on the sphere as a function of time. Assuming triple junctions

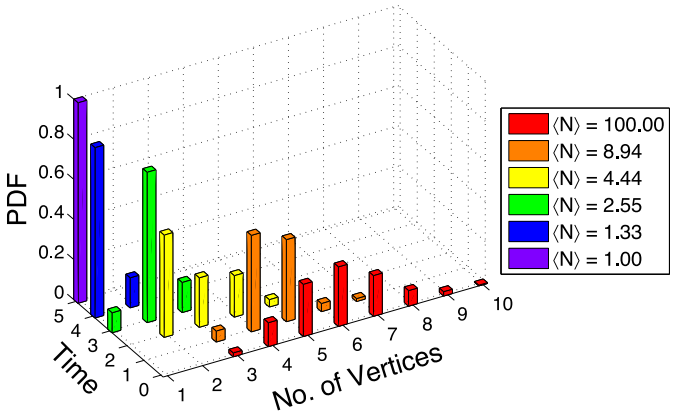

FIG. 8. Probability distribution function for cells with a given number of vertices at different times averaged over 20 simulations. The peak shifts towards cells with smaller numbers of vertices with increasing time.

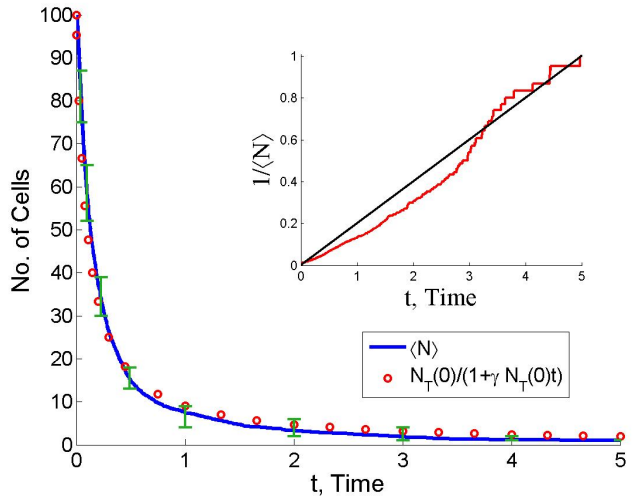

FIG. 9. Total number of cells averaged over 20 simulations as function of time. The simulation data is presented in blue with error bars representing the maximum and minimum number in the simulations. Here $\gamma = .1$ and $N_T(0) = 100$. *Inset:* The inverse of $\langle N \rangle$ as function of time (red).

everywhere and making use of the Euler characteristic of the sphere, one can simply obtain the expression

$$\sum_{n=1}^{\infty} N_n(t) \left(1 - \frac{n}{6}\right) = 2, \tag{22}$$

involving the distribution $N_n(t)$ of $n-$sided cells at time t. From this, one can calculate the total number of cells $N_T(t) = \sum_n N_n(t)$ at time t. The number of cells $N_n(t)$ with n sides can change in two distinct ways: (i) via a boundary flip, where two cells each lose one side and two cells each gain one side and (ii) via cell removal of $2-$, $3-$, and $4-$sided cells. In the former case $N_n(t)$ changes, but the total number $N_T(t)$ does not change, whereas in the latter, some of the $N_n(t)$ values change and the total number $N_T(t)$ decreases by one. We focus therefore on cell removal, where

$$\frac{\partial N_T(t)}{\partial t} = \sum_{n=2,3,4} \frac{\partial N_n^r(t)}{\partial t}, \tag{23}$$

where $\partial N_n^r(t)/\partial t$ is the rate of change of n-sided cells due to cell removal. From Eq. (17) we can estimate the time t_{n0} it takes for the area of an $n-$sided cell to go to zero; $t_{n0} = -\ln\left(1 + \frac{3A_{n0}}{\pi(n-6)}\right) \approx -\frac{3A_{n0}}{\pi(n-6)}$, since the cell areas are small. A crude estimate of the cell area on a unit sphere is $A_{n0} \simeq \frac{4\pi}{N_T(t)}$, and hence the rate of change of the number of n-sided cells is approximately

$$\frac{\partial N_n^r(t)}{\partial t} \approx -\frac{N_n(t)}{t_{n0}} = N_T(t)\frac{N_n(t)(n-6)}{12},$$

and $\frac{\partial N_T(t)}{\partial t} = N_T(t)\sum_{n=2,3,4} \frac{N_n(t)(n-6)}{12}$. As a last step, we take $N_n(t) \simeq \phi_n N_T(t)$ where each ϕ_n is a constant. Then

$$\frac{\partial N_t(t)}{\partial t} = -N_T^2(t)\left(\frac{\phi_2}{3} + \frac{\phi_3}{4} + \frac{\phi_4}{6}\right) = -\gamma N_T^2(t). \tag{24}$$

Solving Eq. (24) gives $N_T(t) = \frac{N_T(0)}{1+\gamma N_T(0)t}$. If we estimate $\gamma = .1$ and the initial number of cells $N_T(0) = 100$, then $N_T(t) = \frac{100}{1+10t}$. This function shows good quantitative agreement with the simulation results shown in Fig. 9. The time evolution of the total number of cells is approximately $N_T \sim 1/t$. At early times, the fraction of cells with less than five sides is approximately 10%, but later the foam is mostly composed of $2-$ and $3-$sided cells, resulting in a larger γ as can be seen in the inset in Fig. 9.

V. V. CONCLUSIONS

In this work, we presented three contributions to the study of foams on curved surfaces.

First, we derived a novel model for the evolution of the foam cell boundaries on a general smooth surface. If the surface is a sphere, then the cell area grows exponentially in time for all times. This differs from the linear growth in the plane. Such exponential growth has been implicitly predicted in [33]; however, the argument used there relied on the assumption of each cell wall having constant geodesic curvature. In fact, cell walls with non-uniform curvature can be observed both in our simulations e.g., Fig. 6, and experiments [34].

Second, to the authors knowledge, this is the first work verifying the theoretical prediction of exponential growth on the sphere. While experimental work in [34] shows that the growth rate differs from linear, our numerical experiments show that the domain growth on the sphere is exponential in time. To test our theoretical predictions we implemented numerical experiments and addressed critical topological events as edges are diminished. The

simulations clearly show exponential growth. In addition, we show that the only stable configuration is the one where a single cell encloses the entire surface of the sphere. Our simulations also suggest that the cell in the initial distribution with the most sides has the highest probability of surviving until the end.

Third, we also provide new results unique to foam coarsening on the sphere: i) the probability distribution of the number of cells with a given number of vertices as a function of time and ii) the prediction and confirmation that the number of cells in the longtime goes as $1/t$.

These observations highlight the insights that our model and simulations provide foam coarsening on the sphere.

VI. ACKNOWLEDGMENTS

ACKNOWLEDGMENTS

The work of all the authors was supported by NSF Grant DMS-1212046. The authors would also like to thank D. Durian, Y. Kim, D. Kinderlehrer, C. S. Peskin, and H. Yokoyama for useful discussions.

[1] J. A. Glazier and D. Weaire. The kinetics of cellular patterns. *J. Phys.: Condens. Matter*, 4:1867–1894, 1992.

[2] M. L. McDermott, M. A. Watsky, D. H. Geroski, and H. F. Edelhauser. A method for the in vitro determination of feline corneal endothelial permeability. *Current Eye Research*, 9(12):1129–1136, 1990.

[3] D. Lindley. Cold dark matter makes an exit. *Nature*, 349:14, 1991.

[4] I. Cantat et al. *Foams: Structure and dynamics*. Oxford University Publishing, 2013.

[5] R. D. James. Materials from mathematics. SIAM News, November 2014.

[6] J. von Neumann. Metal interfaces. In C. Herring, editor, *American Society for Metals*, pages 108–110, Cleveland, 1952.

[7] Y. Kim, M.-C. Lai, and C. S. Peskin. Numerical simulations of two-dimensional foam by the immersed boundary method. *J. Comp. Phys.*, 229:5194–5207, 2010.

[8] D. Weaire and J. P. Kermode. Computer simulation of a two-dimensional soap froth I. method and motivation. *Philosophical Magazine B*, 48(3):245–259, 1983.

[9] D. Weaire and J. P. Kermode. Computer simulation of a tow-dimensional soap froth II. analysis of results. *Philosophical Magazine B*, 50(3), 1984.

[10] J. Wejchert, D. Weaire, and J. P. Kermode. On the distribution of cell areas in a voronoi network. *Philosophical Magazine B*, 53(15), 1986.

[11] T. Herdtle and H. Aref. Numerical experiments on two-dimensional foam. *J. Fluid Mech.*, 241:233–260, 1992.

[12] K. Kawasaki and Y. Enomoto. Statistical theory of ostwald ripening with elastic field interaction. *Physica A*, 150:462, 1988.

[13] K. Kawasaki, T. Nagai, and K. Nakashima. Vertex models for two-dimensional grain growth. *Philosophical Magazine B*, 60:399, 1989.

[14] K. Kawasaki. Aspects of late-stage dynamics of ordering processes. *Physica A*, 163:59, 1990.

[15] D. Kinderlehrer, I. Livshits, and S. Ta'asan. A variational approach to modeling and simulation of grain growth. *SIAM J. Sci. Comput.*, 28(5):1694–1715, 2006.

[16] C. E. Torres, M. Emelianenko, D. Golovaty, D. Kinderlehrer, and S. Ta'asan. Numerical analysis of the vertex models for simulating grain boundary networks. *SIAM J App Math*, 75:762, 2015.

[17] H. Flyvbjerg. Model for coarsening froths and foams. *Physical Review E*, 47(6):4037, 1993.

[18] S. A. Magrabi, B. Z. Dlugogorski, and G. J. Jameson. Bubble size distribution and coarsening of aqueous foams. *Chemical Engineering Science*, 54:4007–4022, 1999.

[19] M. P. Anderson, D. J. Srolovitz, G. S. Grest, and P. S. Sahni. Computer simulation of grain growthI.-V. *Acta Metall.*, 32:783, 1984-1985.

[20] M. P. Anderson, G. S. Grest, and D. J. Srolovitz. Computer simulation of normal grain growth in three dimensions. *Philosophical Magazine B*, 59:293, 1989.

[21] J. A. Glazier, M. P. Anderson, and G. S. Grest. Coarsening in the two-dimensional soap froth and the large-Q Potts model: a detailed comparison. *Philosophical Magazine B*, 62:615, 1990.

[22] E. Holm, J. A. Glazier, D. Srolovitz, and G. S. Grest. . *Physical Review A*, 43:2662, 1991.

[23] S. Hilgenfeldt, A. M. Kraynik, S. A. Koehler, and H. A. Stone. Dynamics of coarsening foams: Accelerated and self-limiting drainage. *Physical Review Letters*, 86(20):4704–4707, 2001.

[24] S. Hilgenfeldt, A. M. Kraynik, D. A. Reinelt, and J. M. Sullivan. The structure of foam cells: Isotropic Plateau polyhedra. *Europhys. Lett.*, 67(3):484–490, 2004.

[25] S. Jurine, S. Cox, and F. Graner. Dry three-dimensional bubbles: Growth-rate, scaling state and correlations. *Colloids and Surfaces A*, 263:18–26, 2005.

[26] D. Weaire and S. Hutzler. *The physics of foams*. Oxford University Press, 2001.

[27] K. A. Brakke. The surface evolver. *Experimental Mathematics*, 1(2):141–165, 1992.

[28] N. Kern, D. Weaire, A. Martin, S. Hutzler, and S. J. Cox. Two-dimensional viscous forth model for foam dynamics. *Physical Review E*, 70:041411, 2004.

[29] R. I. Saye and J. A. Sethian. Multiscale modeling of membrane rearrangement, drainage, and rupture in evolving foams. *Science*, 340:720–724, 2013.

[30] P. Peczak, G. S. Grest, and D. Levine. Monte Carlo studies of grain growth on curved surfaces. *Physical Review E*, 48(6):4470, 1993.

[31] D. Zöllner and P. Streitenberger. Three-dimensional normal grain growth: Monte Carlo Potts model simulation and analytical mean field theory. *Scripta Materialia*, 54:1697–1702, 2006.

[32] G. L. Thomas, R. M. C. de Almeida, and F. Graner. Coarsening of three-dimensional grains in crystals, or

bubbles in dry foams, tends towards a universal statistically scale-invariant regime. *Physical Review E*, 74:021407, 2006.

[33] J. E. Avron and D. Levine. Geometry and foams: 2d dynamics and 3d statistics. *Physical Review Letters*, 69(1):208–211, 1992.

[34] A. E. Roth, C. D. Jones, and D. J. Durian. Coarsening of a two-dimensional foam on a dome. *Physical Review E*, 86:021402, 2012.

[35] A. E. Roth, C. D. Jones, and D. J. Durian. Bubble statistics and coarsening dynamics for quasi-two-dimensional foams with increasing content. *Physical Review E*, 87(4):042304, 2013.

[36] J. Duplat, B. Bossa, and E. Villermaux. On two-dimensional foam ageing. *J. Fluid Mech.*, 673:147–179, 2011.

[37] D. Weaire and N. Rivier. Soap, cells and statistics–random patterns in two dimensions. *Contemp. Phys.*, 25(59), 1984.

[38] W. W. Mullins. Two-dimensional motion of idealized grain boundaries. *J. Applied Physics*, 27(8):900–904, 1956.

[39] J. E. Taylor, J. W. Cahn, and C. A. Handwerker. Overview no. 98: I geometric models of crystal growth. *Acta Metall. Mater.*, 40(7):1443–1474, 1992.

[40] X. Zheng, R. Ennis, G. P. Richards, and P. Palffy-Muhoray. A plane sweep algorithm for the Voronoi tesselation of the sphere. *e-Liquid Crystal Comm.*, 2011.

[41] I. Todhunter. *Spherical Trigonometry*. MacMillan, 1886.

[42] See Suplementary Material at [URL will be inserted by publisher] for the movie showing the evolution of the configuration depicted in Figure 6.

[43] K. Ghalieh and M. Hajja. The Fermat point of a spherical triangle. *The Math. Gazette*, 80(489):561–564, 1996.

[44] I. N. Katz and L. Cooper. Optimal location on a sphere. *Comp. and Maths. with Appls.*, 6:175–196, 1980.

Appendix A: Appendix A: Vertex Evolution

To evolve a vertex $\mathbf{v}$, we solve an alternate problem of finding a point on the sphere which minimizes the sum of the distances to each vertex of the triangle $\{\mathbf{x}_1, \mathbf{x}_2, \mathbf{x}_3\}$ where the points $\mathbf{x}_1, \mathbf{x}_2, \mathbf{x}_3$ are the nearest neighbors of $\mathbf{v}$ along the discretized edges. If all angles are less than $2\pi/3$, then the solution of this problem satisfies the Herring condition [43]. A fixed point iteration scheme was proposed to find such a point in [44] as

$$\mathbf{x}^{k+1} = \frac{\sum_{j=1}^{3} \left\{ \|\mathbf{x}^k - \mathbf{x}_j\|^{-1} \left(1 - \left(\frac{\|\mathbf{x}^k - \mathbf{x}_j\|}{2}\right)^2\right)^{-1/2} \right\} \mathbf{x}_j}{\left\| \sum_{j=1}^{3} \left\{ \|\mathbf{x}^k - \mathbf{x}_j\|^{-1} \left(1 - \left(\frac{\|\mathbf{x}^k - \mathbf{x}_j\|}{2}\right)^2\right)^{-1/2} \right\} \mathbf{x}_j \right\|}. \tag{A1}$$

The initial guess $\mathbf{x}^0$ is taken to be the average of the three neighbors projected back onto the sphere, $\mathbf{x}^0 = (\mathbf{x}_1+\mathbf{x}_2+\mathbf{x}_3)/\|\mathbf{x}_1+\mathbf{x}_2+\mathbf{x}_3\|$. The iterations stop if $\|\mathbf{x}^{k+1}-\mathbf{x}^k\| < \epsilon$ where the tolerance is set to be $\epsilon = 10^{-16}$ in our simulation. With this stopping criterion we achieve convergence within $20-30$ iterations per vertex per time step. After the vertex is computed, we calculate the three angles formed by the new vertex and the nearest edge points and observe numerically that $|\theta - 2\pi/3| \leq 10^{-14}$, thus satisfying the Herring condition. If the triangle formed by the three neighbors has an angle greater than $2\pi/3$, the vertex approaches one of its neighbors upon iteration. In this case, the Herring condition would not be satisfied. To overcome this effect, we simply remove the nearest neighbor $\mathbf{x}_i$ when its angle is greater than $2\pi/3$. This allows the iterations to converge to a point interior to the nearest edge points.